# MODEL TEST OF THE DTI-FLOATING WIND CONCEPT

**J. Serret**, *Floating Wind Turbines Ltd. - IDCORE - University of Edinburgh, UK*
**T. Tezdogan**, *University of Strathclyde, UK*
**T. Stratford**, *University of Edinburgh, UK*
**P. R. Thies**, *University of Exeter, UK*
**V. Venugopal**, *University of Edinburgh, UK*

## ABSTRACT

This study aims to de-risk the development of the Deep Turbine Installation-Floating (DTI-F) concept, a hybrid spar buoy-based floating offshore wind turbine with the novelty of being able to raise up and lower down the tower plus nacelle set. The paper presents the design and construction of a Froude-scaled model based on the DTI-F concept, the experimental testing configurations and conditions, and the instrumentation used to measure motions and loads. The test campaign included free decay and stiffness decay tests, along with regular and irregular wave testing. In addition to the hydrodynamic characterisation, the resonance properties of the system with different mooring configurations, i.e. three and four lines, and three lines with a delta connection, were investigated. We present the Response Amplitude Operators (RAOs) in all 6 degrees of freedom for two different mooring configurations. This work is the first step towards the calibration and performance improvement for existing numerical models of the DTI-F concept.

## NOMENCLATURE

| | |
|---|---|
| FOWT | Floating Offshore Wind Turbine |
| DTI-F | Deep Turbine Installation-Floating |
| RAO | Response Amplitude Operator |
| NOTF | National Ocean Test Facility |
| OERF | Ocean Energy Research Facility |
| $H_s$ | Significant height |
| $T_p$ | Peak wave period |
| $H_{max}$ | Maximum wave height |
| $H$ | Height |
| $W$ | Width |
| $L$ | Length |
| Ø | Diameter |
| CoG | Center of gravity |
| $Iîî$ | Moment of inertia in îî direction |
| DoF | Degree of freedom |
| NaN | Not a number |
| FFT | Fast Fourier Transform |
| JONSWAP | Joint North Sea Wave Observation Project |

## 1. INTRODUCTION

Offshore wind in deeper water will be an increasing source of renewable energy over the next few years, and floating wind turbines have the potential to play an essential role in the future energy mix. Hitherto, different floating foundations have been proposed [1, 2].

The floating concept that has been most extensively tested is the spar buoy-based Floating Offshore Wind Turbine (FOWT). In particular, Statoil [3] installed their first full-scale spar buoy FOWT back in 2009 in the North Sea which became the world's first floating wind farm producing electric power [4].

The offshore renewable energy industry utilises various numerical tools to face such complex designs [5]; however, as floating wind is an emerging technology, any numerical development must be validated against testing results.

This paper details the design and construction of a 1:45 Froude scaled model of the DTI-F wind concept, and describes the experimental testing performed at Lir National Ocean Test Facility (NOTF) and FloWave Ocean Energy Research Facility (OERF). The overall aim of the test campaign was to obtain suitable data for the hydrodynamic characterisation of the DTI-F concept.

The specific objective of this study is to validate the initial design by ensuring that natural periods of the structure are not within the range of periods that occur in the common sea states. An additional objective of the experimental testing was to evaluate the advantages and disadvantages of three different mooring configurations.

## 2. EXPERIMENTAL SET-UP

This section presents a summary of the properties of the basin, the scaled model along with the instrumentation, and the mooring system tested.

### 2.1 TEST FACILITY

The testing was carried out in the Ocean Wave Basin of the Lir NOTF in Cork (Ireland). The basin (Figure 1) is 15.14 m long, 25.85 m wide. It has an 11.2 m × 10 m deep section equipped with a movable floor plate. The working water depth was set to 2 m to conduct the testing.

Figure 1 Ocean Wave Basin at Lir National Ocean Test Facility

The basin is equipped with 80-hinged paddles located on two sides of the basin allowing for adjustable wave directions. The paddles can generate peak wave conditions with a significant wave height of $H_s$=0.16 m, peak wave period of $T_p$=1.4 s, and $H_{max}$=0.32 m, which make it ideal to test operational conditions for 1:45 scaled models such as the one considered in this study.
The software to generate the sea structure is Njord Wave Synthesiser, a wave code from Edinburgh Designs Ltd, who are also the designers of the basin.

### 2.2 MODEL DESCRIPTION

A 1:45 model was machined and assembled (Figure 2) in the FloWave OERF workshop, using geometrically-scaled dimensions from the full-scale DTI-F. The model was constructed of divinycell closed cell foam sections with aluminium interface and heave plates (Figure 3). Fixed steel ballast was located in the lower section of the model. The design allowed for approximately 10 kg of moveable ballast in the upper cylinder to fine-tune the final draft and centre of gravity.

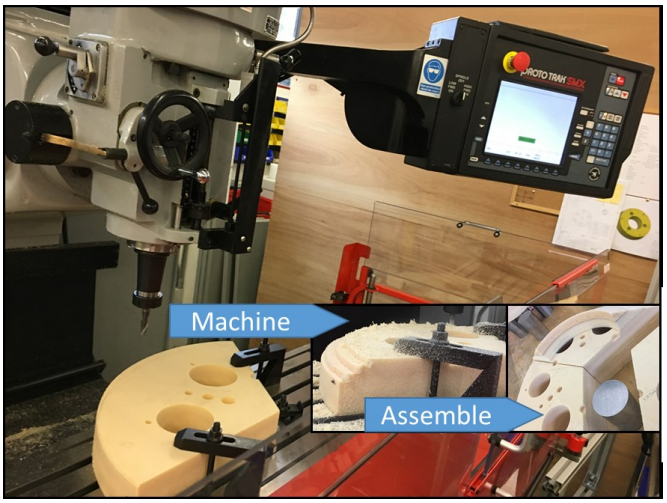


Figure 2 Milling machine ready to cut a piece, working on the frustum, and a view showing how some of the pieces were assembled

The scale model was designed to preserve the Froude hydrodynamic similitude. Hence it maintains Froude and Keulegan-Carpenter numbers but does not preserve Reynolds, Weber, and Strouhal numbers. Table 1 presents the dimensions of the scaled model and Table 2 shows the mass properties of the manufactured model and the percentage difference with the target values. The tower and nacelle were modelled to match the mass distributions of the Levenmouth (Samsung Heavy Industries - S7.0-171) demonstration foreshore wind turbine as described in [6].

**Table 1 DTI-F scaled to 1:45**

| | *H* (mm) | *W* (mm) | *L* (mm) | *Ø* (mm) |
|---|---|---|---|---|
| DTI-F | 3651 | - | - | - |
| Tip mass | 200 | 178 | 556 | - |
| Tower | 1628 | - | - | 156 |
| Top cylinder | 1556 | - | - | 333 |
| Frustum | 111 | - | - | - |
| Base cylinder | 111 | - | - | 667 |
| Heave plate | 44 | - | - | 889 |

**Table 2 DTI-F mass properties scaled to 1:45 and difference with the target values.**

| | Mass (kg) | CoG Z (mm) | Ixx ($kgm^2$) | Iyy ($kgm^2$) | Izz ($kgm^2$) |
|---|---|---|---|---|---|
| Model | 186 | 447 | 126 | 126 | 10 |
| % | 0 | 0 | 8 | 8 | -5 |

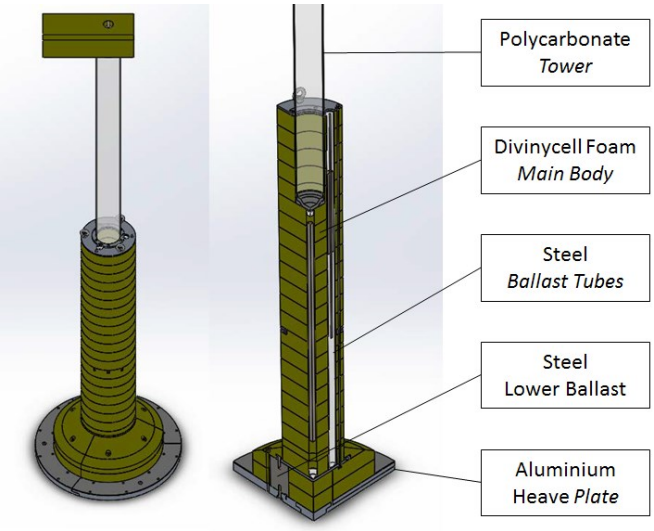


Figure 3 Manufacture design of the DTI-F. The drawing on the right is a quadrant showing the inner structure

## 2.3 MOORING SYSTEM

The laboratory testing includes three different configurations using catenary lines: (a) three mooring lines, (b) four mooring lines, and (c) three mooring lines, but with a delta connection. The layout is shown in Figure 4 (the delta connection setup uses the three line layout). It also presents the position of the movable floor, shown as a square. Tables 3 and 4 provide the position of the fairleads for the three and four mooring layout respectively. The origin of the measurements is located in the bottom-centre of the heave plate, i.e. the corner depicted in the drawing on the right of Figure 3.

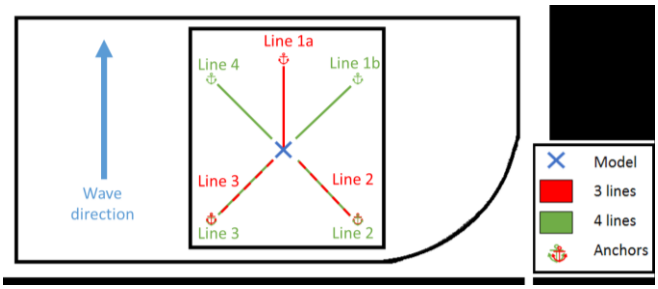


Figure 4 Mooring layout for the different configurations

**Table 3 Fairleads position for the three mooring layout**

| | x (mm) | y (mm) | z (mm) |
|---|---|---|---|
| Line 1a | 167 | 0 | 822 |
| Line 2 | -83 | 144 | 822 |
| Line 3 | -83 | -144 | 822 |

**Table 4 Fairleads position for the four mooring layout**

| | x (mm) | y (mm) | z (mm) |
|---|---|---|---|
| Line 1b | 167 | 0 | 822 |
| Line 2 | 0 | 167 | 822 |
| Line 3 | -167 | 0 | 822 |
| Line 4 | 0 | -167 | 822 |

When the three mooring line configuration is used, the angle between the lines is kept at 120 degrees. For the four mooring line configuration, the anchoring points are spread at 90 degrees. However, due to model restrictions, the fairleads were distributed symmetrically at 60 and 120 degrees as shown in Figure 5.

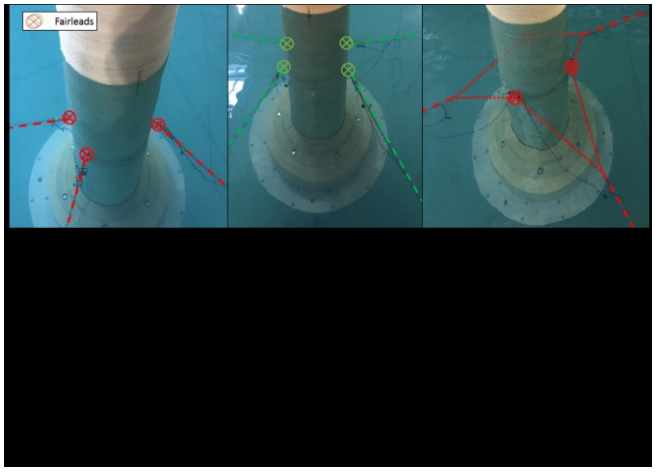


Figure 5 Mooring lines view and fairlead positions

The delta connection takes advantage of the position of the three mooring line configuration fairleads as depicted in Figure 6. The delta lines are connected to the mooring line with a shackle. A load cell is installed between the shackle and the mooring line to measure the force in the mooring line. This configuration was tested to investigate the benefits of having greater yaw stiffness.

The weight per unit length in the water and the length of the mooring line are the most relevant mooring line parameters for the floating structure response.

Tables 5 and 6 show the scaled mooring configurations for the three and four mooring setups, and Table 7 provides the features of the mentioned chains. The delta configuration is identical to the three mooring configuration but including the weight of the delta connection, i.e. 0.05 kg.

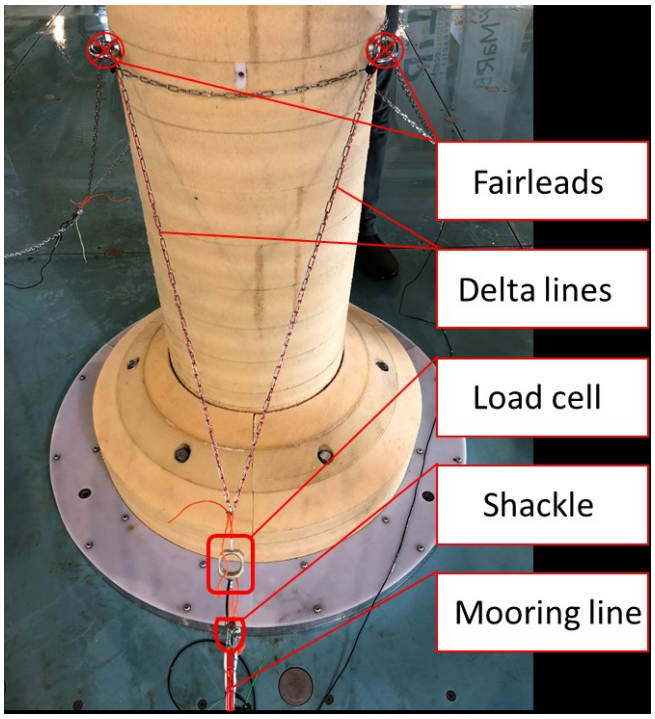

Figure 6 Detail of the delta connection setup

**Table 5 Mooring features for the three mooring configuration**

| | 622 Chain (m) | 155 Chain (m) | Shackles (-) | Links (-) |
|---|---|---|---|---|
| Line 1a | 5.00 | 0.00 | 2 | 0 |
| Line 2 | 1.56 | 3.70 | 2 | 2 |
| Line 3 | 1.56 | 3.70 | 2 | 2 |

**Table 6 Mooring features for the four mooring configuration**

| | 622 Chain (m) | 155 Chain (m) | 151 Chain (m) | Shackles (-) | Links (-) |
|---|---|---|---|---|---|
| Line 1b | 1.56 | 0.00 | 3.70 | 2 | 2 |
| Line 2 | 1.56 | 3.70 | 0.00 | 2 | 2 |
| Line 3 | 1.56 | 3.70 | 0.00 | 2 | 2 |
| Line 4 | 1.56 | 0.00 | 3.70 | 2 | 2 |

Combining the information provided regarding the mooring lines, Line 1a, i.e. three lines setup; has 5.04 m and 1.42 kg. Line 1b, i.e. four lines setup; has 5.35 m and 1.01 kg, Line 2 has 5.35 m and 1.01 kg, Line 3 has 5.08 m and 1.07 kg, and Line 4 has 5.06 m and 1.07 kg. To characterise the mooring lines completely, an additional 0.44 m and 0.4 kg have to be taken into account when using the delta connection. Similarly, 0.26 m and 0.39 kg have to be added when using the four mooring lines configuration.

**Table 7 Features of the different components of the mooring lines**

| | Weight |
|---|---|
| 622 Stain Steel Chain | 0.27 kg/m |
| 155 Stain Steel Chain | 0.21 kg/m |
| 151 Stain Steel Chain | 0.20 kg/m |
| Δ Stain Steel Chain | 0.03 kg/m |
| Stain Steel Shackles | 0.10 kg |
| Stain Steel Links | 0.10 kg |

## 2.4 INSTRUMENTATION

The instrumentation listed below was used during the testing, to measure the wave surface elevations in the tank, the loads in the mooring lines, and the motions of the floating platform:

- The generated wave heights were measured using six resistive twin-wire probes, connected to a Churchill control amplifier.
- The six degree of freedom (DOF) motions of the floating platform were measured using an optical tracking system, Qualisys ProReflex MCU.
- The mooring line tensions were measured using four force transducers located between the fairleads and the mooring line. For the delta connection configuration, the transducers were installed between the delta lines and the mooring line as shown in Figure 6. The weight of the submersible s-beam load cells is 8.5 g, and their capacity is 22.2 Newton.

## 2.5 TEST MATRIX

A comprehensive test programme was prepared to characterise the DTI-F concept completely. It covered free and stiffness decay, regular and irregular seas, and some special tests. This paper deals only with regular wave tests. Table 8 outlines the experiments conducted during the testing. Free decay tests were performed for heave, pitch, and roll motions. Stiffness decay tests were carried out for all six DoF, and for three and four mooring line configurations.

**Table 8 Test programme**

| Type of tests | Number of tests |
|---|---|
| Free decay tests | 9 |
| Stiffness decay tests | 36 |
| Regular wave tests | 88 |

## 2.6 TESTING CONDITIONS

Different wave conditions were tested to characterise the response of the floating system. Twenty-two regular wave tests were carried out, covering wave periods from 0.70 to 2.24 seconds and wave amplitudes of 44 and 110 millimetres, and three irregular waves matching the conditions of a possible deploying area at Buchan Deep Demonstration Site [7].

The frequency quality of the waves delivered by the testing facility is shown in Figure 7. In general, the wave quality is acceptable to perform further investigations. However, there is a poorer match in the higher frequencies of the irregular seas and the higher frequency of the 44 millimetres amplitude regular wave. Figure 8 presents a comparison of the experimental wave versus target wave for two different regular waves with wave amplitudes of 44 and 110 millimetres.

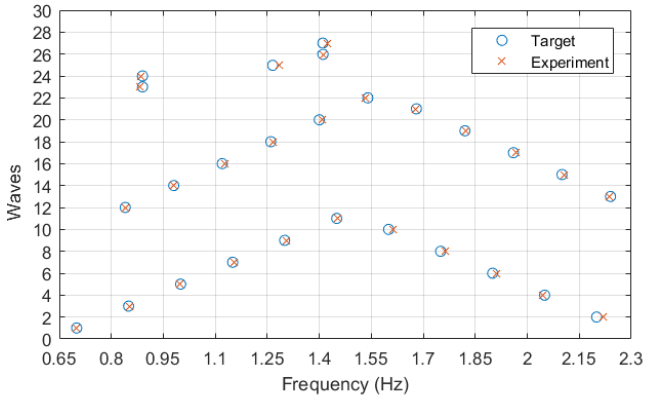


Figure 7 Frequency wave quality at Lit NOTF

It has been found that the experimental wave height is smaller than the target. The 44-millimetre waves were off by 23% for low frequencies arising until 27% for higher frequencies. The 110-millimetre waves present a 10% discrepancy with the target for low frequencies while for higher frequencies the experimental wave matches the target adequately. This behaviour regarding wave height seems to be a constant for the basins designed by Edinburgh Designs [8].

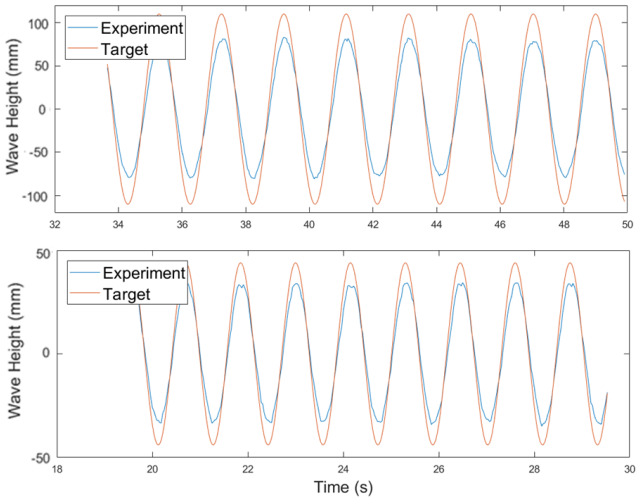


Figure 8 Comparison of the experimental wave and target wave. The figure in the bottom shows the wave amplitude of 44 mm, and the figure at the top shows a wave of amplitude of 110 mm

Correct wave simulation is critical to obtain the RAOs at desired frequencies. The accuracy and precision of a basin when reproducing waves at particular frequencies defines its usability when more accurate results are needed, and ensures reliable conclusions.

# 3. PRE-PROCESSING

This section provides an overview of the methods applied in this study to pre-process the test data. Pre-processing includes data selection, cleaning, transformation, and filtering of the data, which is shortly described in the following.

Data selection is applied for reducing the original data set to the useful values. In the measured time series data, the first oscillation was excluded from the decay test results, as moving the model into an offset position and releasing it may introduce additional damping. In general, ignoring the start-up of each time series avoids transient effects, which is a crucial factor to get reliable results. At least ten oscillations were included in the time window, to produce reliable averages.

All the time series must be cleaned to interpolate corrupt points and correct erroneous data, i.e. infinite and not a number (NaN). The raw data was not deleted though, since keeping corrupt and erroneous data leads to less error than merely removing them [9].

Data transformation is an important step to analyse testing results. It includes processes like detrending and normalisation. The Matlab *Detrend*

function computes the least-squares fit of a straight line to the data and removes the linear trend from a set of data. This step is relevant for Fast Fourier Transform (FFT) processing since it helps to minimise the effect of the approximation made when cutting up the signal into finite-lengths segments to compute the FFT. Normalisation is the transformation of a set of data into its canonical form to minimise redundancy and dependency.

Even for still-water phenomena, there are oscillations in the records, i.e. noise. Therefore, the appropriate filters must be applied to account for undesirable measurements. Note that sensor related unphysical noise is already removed by the acquisition hardware.

Other sources of noise can be transients, structural vibrations, and experimental errors. There is a wide variety of post-processing errors. However, transient related errors are typically low-frequency noises, and structural vibrations are high-frequency noises. Consequently, they can be mitigated by using high-pass and low-pass filters respectively. The choice of filters for this study comprises two different kinds of smoothing and an interval-dependent denoising filter.

The *Smooth* function is a moving average lowpass with filter coefficients equal to the reciprocal of the span to be averaged. Whereas the *Savitzky-Golay filter* is a generalised moving average with filter coefficients determined by an unweighted linear least-squares regression and a fourth polynomial model [10].

In practice, the *Savitzky-Golay filter* smooths the input signal but being more faithful to the original signal than the *Smooth* filter.

The interval-dependent denoising filter, also called *1-D stationary wavelet function*, performs a multilevel one-dimensional wavelet analysis using *db3* wavelet decomposition filters.

As depicted in Figure 9, the detrending process only sets the origin at zero while removing the drift from the time series. The bottom subplots present a zoom of the red box marked in the top ones to show the effect of the different smoothing strategies.

As shown in Figure 10, the wavelet decomposition filter returns a very smooth signal, although the filter can fit small peaks during the smoothing process.

Depending on the original data and the expected outcome, the most appropriate combination of the pre-processes previously presented are chosen. Care needs to be taken when performing signal pre-processing to ensure that it introduces no extra source of error.

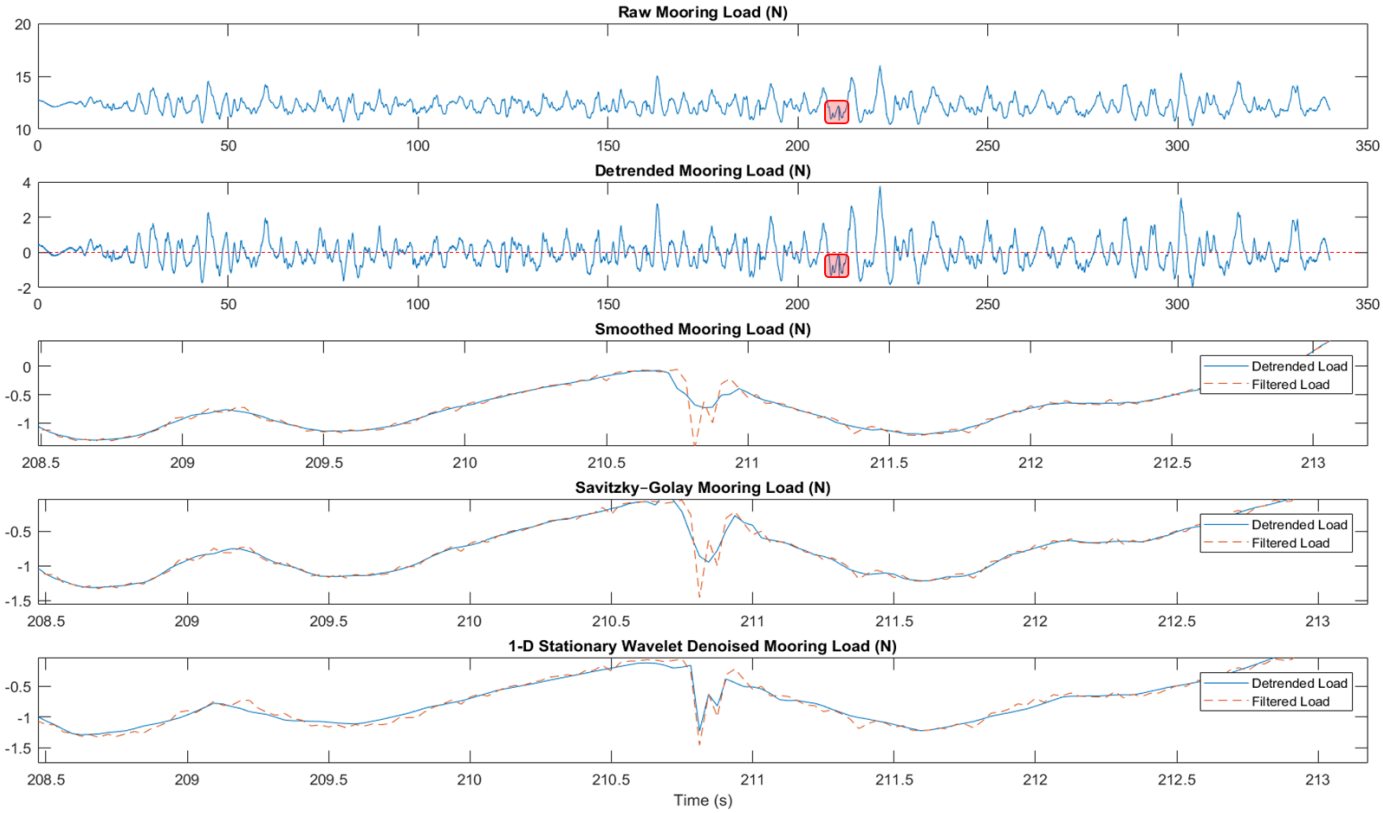


Figure 9 Different filter types used in this study

## 4. FREE DECAY TESTS

Free decay tests in heave, pitch and roll modes of motion were carried out to investigate the resonance properties and the hydrodynamic coefficients of the system. Each set of tests was repeated three times to check for experimental bias. These experiments were conducted by applying a prescribed displacement in heave, pitch and roll from the stationary equilibrium position, and cautiously releasing it. Figure 10 presents an overview of the typical record coming from a heave free decay test including the other motions. It is essential to verify that the magnitude of the tested motion is larger than the other modes of motion to ensure that most of the energy within the system has been employed to produce the tested motion. To compute damping coefficients and natural frequencies, the procedure explained in [11] has been followed. The properties of the oscillating system, i.e. logarithmic decrement and natural frequency, have been calculated by means of two different sets of calculated data. The first set of results includes the logarithmic decrement determined from the fitting of an exponential curve (Figure 11). The peaks shown in Figure 11 come from the peak finding process (Figure 12) of the oscillation motion.

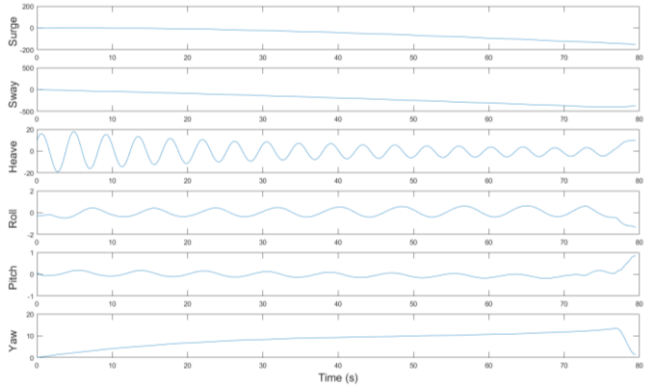


Figure 10 Heave free decay test results. Translational motions in millimetres and rotational in degrees

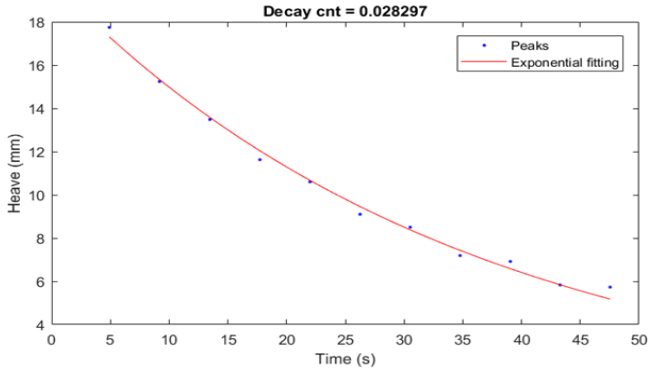


Figure 11 Exponential fitting of the peaks of the heave free decay test

This set of data also uses the oscillation period computed from the peak finding process to calculate the heave natural frequency.
The second set of results involves the logarithmic decrement and natural frequency estimated during the fitting of the damped sinusoidal heave response (Figure 12).

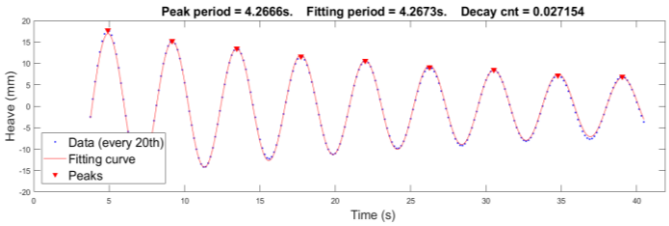


Figure 12 Damped sinusoidal fitting and peak finding of the motion response during the heave free decay test

Table 9 presents the results of the three heave free decay tests that were performed in order to show testing repeatability and reproducibility. No remarkable differences were found between the two methods used to produce the results.

**Table 9 Heave free decay tests results**

| | Damping Coefficient (-) | | Natural Frequency (Hz) | |
|---|---|---|---|---|
| | Set 1 | Set 2 | Set 1 | Set 2 |
| Test 1 | 0.005 | 0.004 | 1.473 | 1.473 |
| Test 2 | 0.004 | 0.004 | 1.473 | 1.477 |
| Test 3 | 0.004 | 0.004 | 1.477 | 1.477 |

A similar process was applied to the other translational degrees of freedoms to determine their damping and natural frequencies. Table 10 shows the summary of the results for all the free decay tests.

**Table 10 Free decay tests results**

| | Damping Coefficient (-) | Natural Frequency (Hz) |
|---|---|---|
| Heave | 0.004 | 1.475 |
| Pitch | 0.001 | 0.768 |
| Roll | 0.002 | 0.769 |

## 5. STIFFNESS DECAY TESTS

Stiffness decay tests in heave, surge, sway, yaw, pitch, and roll modes of motion were carried out to investigate the behaviour of the mooring system.

Again, each set of experiments was repeated three times to check for experimental bias. The experiments were conducted by applying a prescribed displacement in the mode of motion to study, displacing the floater from the stationary equilibrium position, and then cautiously releasing it. Figure 13 shows a typical record from a heave stiffness decay test.

Since the facility lacks a footbridge, the excitation was exerted from a boat. It is worth noting the effect of the boat movement at the beginning the record in the sixth time series labelled WP for wave probe.

Using the same procedure outlined for analysing free decay tests, the natural frequencies and damping coefficients for the floating system including the mooring lines were calculated. The results are presented in Table 11. Note that the natural periods (in seconds) of the last three columns of the table correspond to the values of the full-scale structure to allow for a proper comparison.

Chabaud [9] discusses the difficulty of carrying out pitch and heave tests. Oguz *et al.* [12] carried out surge and pitch, and Sethuraman and Venugopal [13] performed surge, heave and pitch stiffness decay tests. Therefore, there is no apparent justification for the fact that surge results were not conclusive for the four mooring line and the delta connection configurations.

## 6. REGULAR WAVE TESTS

Regular wave tests aim to evaluate the behaviour of the system in a controlled environment by assessing the RAOs. RAO is a non-dimensional transfer function relating the wave elevation ($\eta_i$) and the motion response ($\zeta_i$) for the $i^{th}$ degree of freedom and is given by:

$$RAO_i(w) = \frac{\zeta_i(w)}{\eta_i(w)} \qquad (1)$$

Figure 14 shows a full set of records for a regular wave test with an amplitude of 44 millimetres and a period of 0.70 seconds.

It should be noted the mooring response in the form of regular cycles overlapped in the record of the different modes of motion.

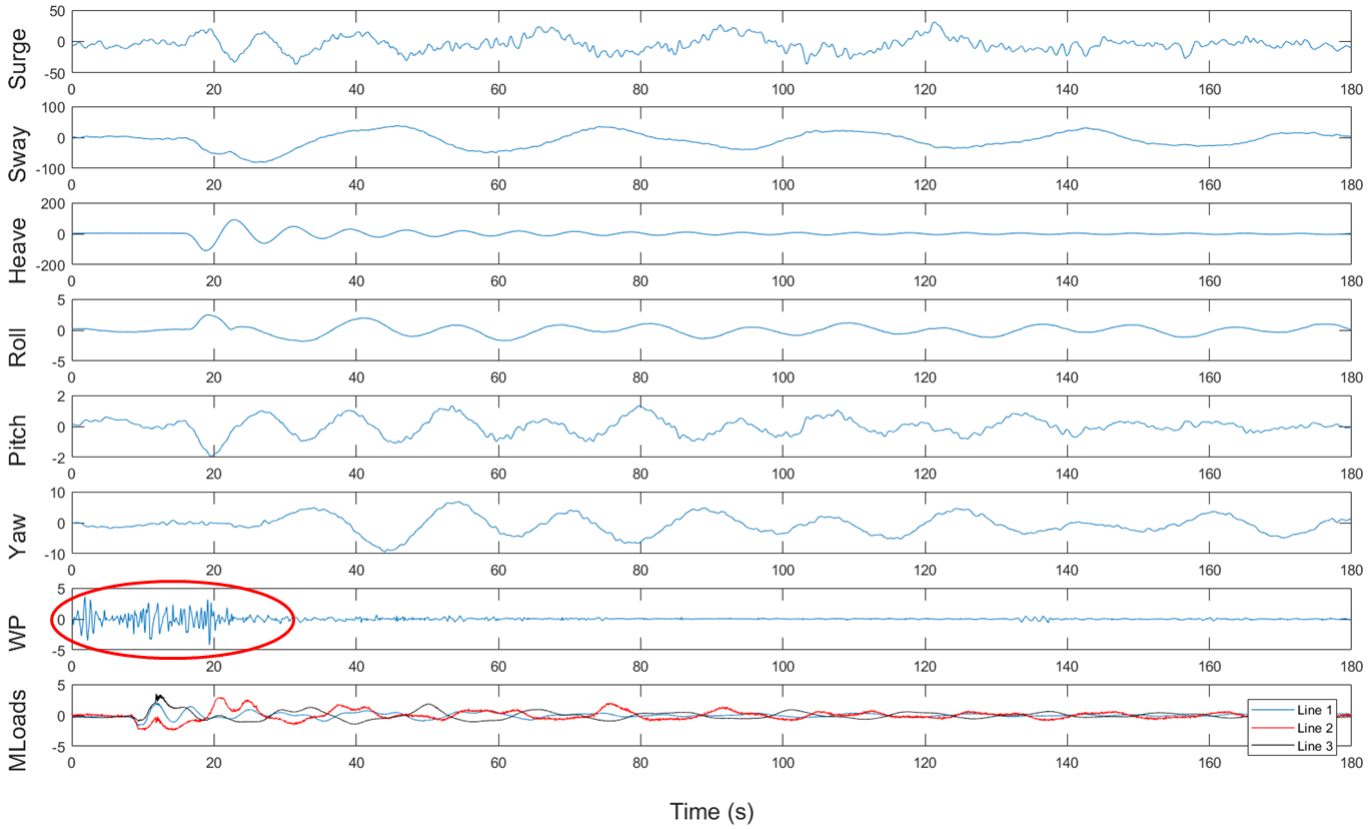


Figure 13 Full set of results of a heave stiffness decay test. Translational motions in millimetres and rotational in degrees, water probe in millimetres and loads in Newton

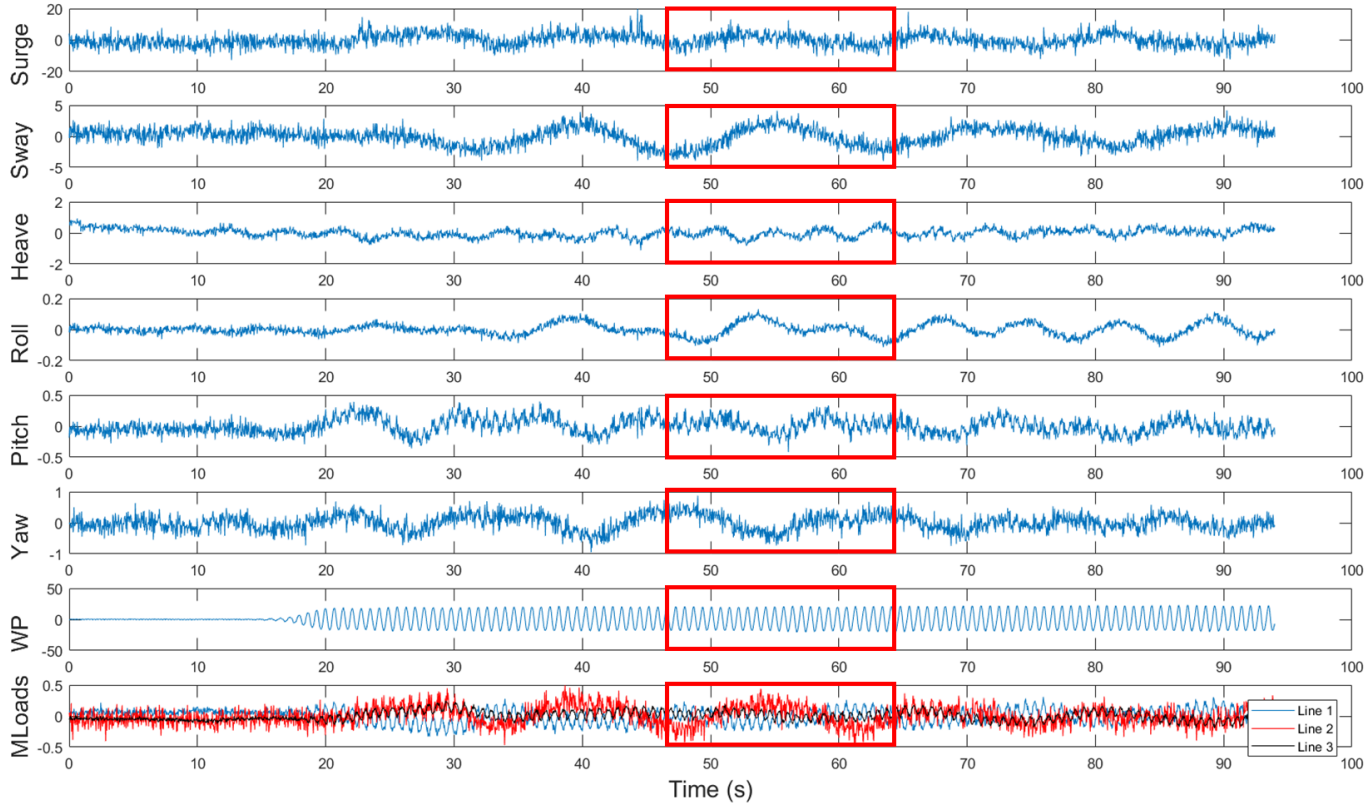


Figure 14 Full set of records for a regular wave test. Translational motions in millimetres and rotational in degrees, water probe in millimetres and loads in Newton

**Table 11 Stiffness decay tests results**

| | Damping Coefficient (-) | | | Natural Frequency (Hz) | | | Natural Period (s) | | |
|---|---|---|---|---|---|---|---|---|---|
| Mooring setup | 3 | Δ | 4 | 3 | Δ | 4 | 3 | Δ | 4 |
| Heave | 0.004 | 0.004 | 0.004 | 1.495 | 1.495 | 1.495 | 28 | 28 | 28 |
| Surge | 0.002 | * | * | 0.249 | * | * | 169 | * | * |
| Sway | * | * | * | * | * | * | * | * | * |
| Pitch | 0.001 | 0.001 | 0.001 | 0.48 | 0.768 | 0.851 | 88 | 55 | 50 |
| Roll | 0.001 | 0.002 | 0.001 | 0.461 | 0.769 | 0.865 | 91 | 55 | 49 |
| Yaw | 0.001 | 0.005 | 0.002 | 0.348 | 1.012 | 0.605 | 121 | 42 | 70 |
| * Inconclusive results | | | | | | | | | |

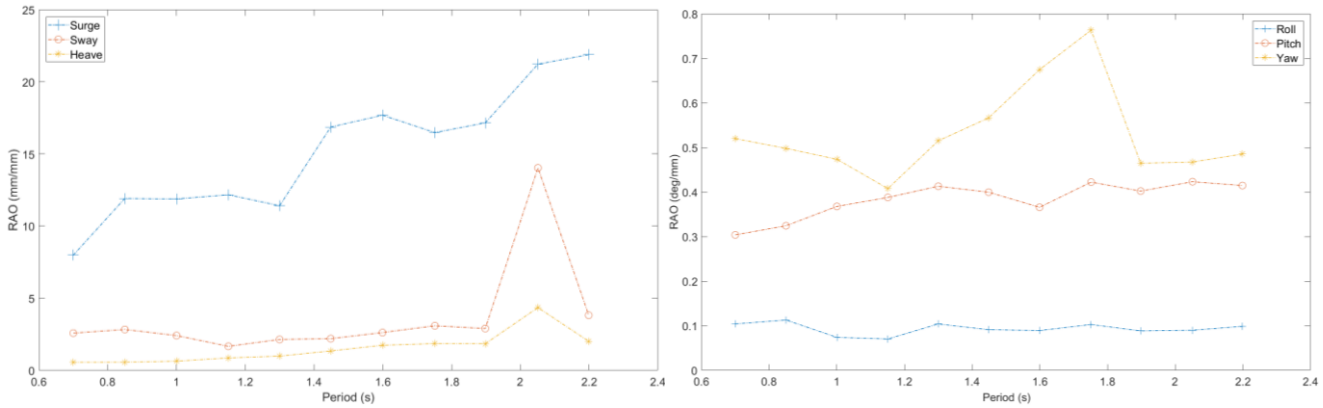


Figure 15 The RAO of translational (left) and rotational (right) motions for three mooring lines

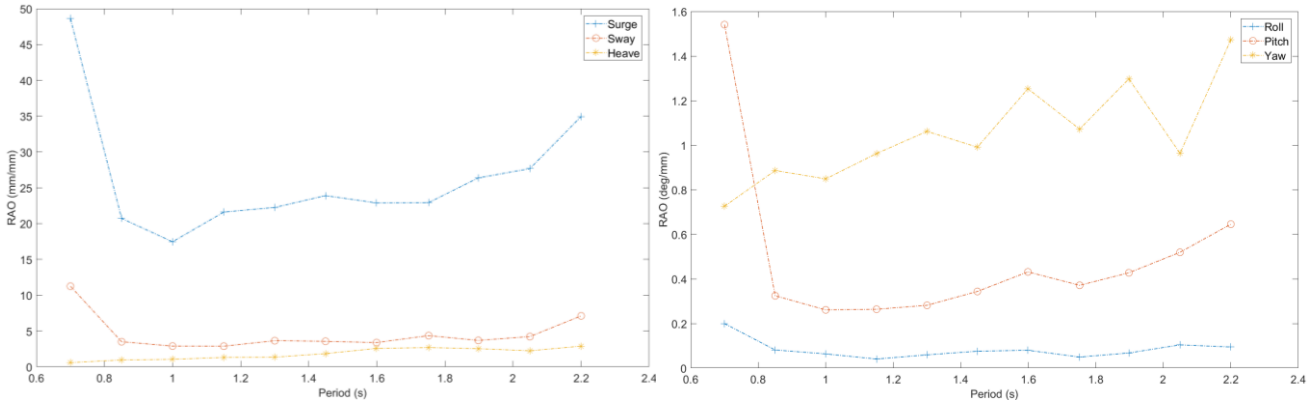

Figure 16 The RAO of translational (left) and rotational (right) motions for four mooring line

Surge and sway modes of motion (the first and second time series in Figure 14) present clear and regular cycles directly related to the oscillations found in the load response of the first and second mooring lines. Heave mode of motion (the third time series in Figure 14) presents four smaller amplitude cycles in the same spam. Roll and pitch modes, on the other hand, exhibit a strong coupling between the mooring lines as depicted in the fourth and fifth time series, shown in Figure 14. The yaw rotational mode of motion (the sixth time series in Figure 14) presents the same cycle shown in surge and sway but with 180 degrees phase shift, matching the load response of the third mooring line.

Figures 15 and 16 present the RAOs for three and four mooring line configurations. The higher number of lines restraints the system in the translational motions, but increases the response in the rotational DoFs. The results also show that considerable excitation occurs only in the surge and sway modes of motion.

## 7. CONCLUSIONS

This study describes model tests for the DTI-F concept and presents the resonance properties and RAOs of the system with different mooring configurations.

The free decay tests characterise the DTI-F system hydrodynamically, and stiffness decay tests results show that all six DoF motion natural periods are longer than the linear wave excitation since the ocean waves contain first harmonic wave energy in the period range of 5 - 25 seconds. For a spar buoy-based FOWT the natural periods in surge, sway and yaw should be more than 100 seconds. Natural periods in heave should be in the period range 20-35 seconds, whereas roll and pitch should be between 50-90 seconds [14]. Therefore, the results meet the constraints specified in the relevant standards.

Comparing those results with the Statoil's Hywind project results [15, 16], the DTI-F concept has a 25% longer surge period, a similar heave period, a 75% longer pitch and roll periods, and a 95% longer yaw period.

Regarding regular tests, more testing is needed to characterise the RAOs of the system completely.

## ACKNOWLEDGEMENTS

This work has received support from:

- MaRINET2 - European Union's Horizon 2020 research and innovation programme under grant agreement number 731084.
- Floating Wind Turbines Limited (FWT Ltd).
- The Energy Technologies Institute (ETI); Research Councils UK (RCUK); Energy Programme for the Industrial Doctorate Centre for Offshore Renewable Energy (IDCORE) [grant number EP/J500847/1].

## REFERENCES

1. The Carbon Trust (2015). Market and Technology Review. Floating Offshore Wind. [online] Available at: https://www.carbontrust.com/media/670664/floating-offshore-wind-market-technology-review.pdf [Accessed 20 May 2018].

2. European Wind Energy Association (2013). Deep Water. The next step for offshore wind energy. [online] Available at: http://www.ewea.org/fileadmin/files/library/publications/reports/Deep_Water.pdf [Accessed 20 May 2018].

3. Equinor.com. (2018). Our offshore wind projects - Our offshore wind projects - equinor.com. [online] Available at: https://www.equinor.com/en/what-we-do/new-energy-solutions/our-offshore-wind-projects.html [Accessed 20 May 2018].

4. WindEurope. (2018). A breakthrough for offshore wind: world's first floating wind farm opens in Scotland | WindEurope. [online] Available at: https://windeurope.org/newsroom/news/a-breakthrough-for-offshore-wind-worlds-first-floating-wind-farm-opens-in-scotland/ [Accessed 20 May 2018].

5. Nielsen, F., Hanson, T. and Skaare, B. (2006). Integrated Dynamic Analysis of Floating Offshore Wind Turbines. Proceedings of 25th OMAE. [online] Available at: http://citeseerx.ist.psu.edu/viewdoc/download?doi=10.1.1.467.4491&rep=rep1&type=pdf [Accessed 20 May 2018].

6. Serret, J. (2018). Code comparison of a NREL-FAST model of the Levenmouth wind turbine with the GH Bladed commissioning results. Proceedings of the ASME 2018 37th International Conference on Ocean, Offshore and Arctic Engineering.

7. Statoil ASA (2015). Environmental Statement. Hywind Scotland Pilot Park. [online] Available at: http://marine.gov.scot/datafiles/lot/hywind/Environmental_Statement/Non-technical_summary.pdf [Accessed 25 May 2018].

8. Venugopal, V., 'EngD advisory meeting' [interviewed by Jordi Serret], 01 June 2018, Jordi Serret IDCORE EngD candidate, University of Edinburgh, Kings Building, Edinburgh.

9. Chabaud, V. (n.d.). Experimental Methods in Marine Hydrodynamics - Lecture in week 36.

10. Uk.mathworks.com. (2018). Smoothing and Denoising- MATLAB & Simulink- MathWorks United Kingdom. [online] Available at: https://uk.mathworks.com/help/signal/smoothing-and-denoising.html?searchHighlight=smooth%20Savitzky-Golay%20filter&s_tid=doc_srchtitle [Accessed 20 May 2018].

11. Brown.edu. (2018). Dynamics and Vibrations: Notes: Free Damped Vibrations. [online] Available at: https://www.brown.edu/Departments/Engineering/Courses/En4/Notes/vibrations_free_damped/vibrations_free_damped.htm

12. Oguz, E., Clelland, D., Day, A., Incecik, A., López, J., Sánchez, G. and Almeria, G. (2018). Experimental and numerical analysis of a TLP floating offshore wind turbine. Ocean Engineering, 147, pp.591-605.

13. Sethuraman, L. and Venugopal, V. (2013). Hydrodynamic response of a stepped-spar floating wind turbine: Numerical modelling and tank testing. Renewable Energy, 52, pp.160-174.

14. DNV Recommended Practice DNV-RP-F205, Global Performance Analysis of Deepwater Floating Structures, October 2010

15. Driscoll, F., Jonkman, J., Robertson, A., Sirnivas, S., Skaare, B. and Nielsen, F. (2016). Validation of a FAST Model of the Statoil-hywind Demo Floating Wind Turbine. Energy Procedia, 94, pp.3-19.

16. Skaare, B., Nielsen, F., Hanson, T., Yttervik, R., Havmøller, O. and Rekdal, A. (2014). Analysis of measurements and simulations from the Hywind Demo floating wind turbine. Wind Energy, 18(6), pp.1105-1122.